Chinese Chemical Letters 32 (2021) 1998–2004

Contents lists available at ScienceDirect

Chinese Chemical Letters

journal homepage: www.elsevier.com/locate/cclet

Communication

A facile construction of heterostructured ZnO/Co_3O_4 mesoporous spheres and superior acetone sensing performance

Mengli Lei[a], Xinran Zhou[a], Yidong Zou[b,**], Junhao Ma[a], Fahad A. Alharthi[c], Abdulaziz Alghamdi[c], Xuanyu Yang[a], Yonghui Deng[a,d,*]

[a] *Department of Chemistry, State Key Laboratory of Molecular Engineering of Polymers, Shanghai Key Laboratory of Molecular Catalysis and Innovative Materials, iChEM, Fudan University, Shanghai 200433, China*
[b] *Institute of Translational Medicine, Shanghai University, Shanghai 200444, China*
[c] *Department of Chemistry, College of Science, King Saud University, P.O. Box 2455, Riyadh 11451, Saudi Arabia*
[d] *State Key Lab of Transducer Technology, Shanghai Institute of Microsystem and Information Technology, Chinese Academy of Sciences, Shanghai 200050, China*

ARTICLE INFO

Article history:
Received 29 September 2020
Received in revised form 21 October 2020
Accepted 28 October 2020
Available online 29 October 2020

Keywords:
Mesoporous materials
P-N heterojunction
Nanocrystal
Nano-size effect
Gas sensing

ABSTRACT

The rapid development of internet and internet of things brings new opportunities for the expansion of intelligent sensors, and acetone as a major disease detection indicator (*i.e.*, diabetes) making it become extremely important clinical indicator. Herein, uniform mesoporous ZnO spheres were successfully synthesized *via* novel formaldehyde-assisted metal-ligand crosslinking strategy. In order to adjust the pore structure of mesoporous ZnO, various mesoporous ZnO spheres were synthesized by changing weight percentage of $Zn(NO_3)_2{\cdot}6H_2O$ to tannic acid (TA). Moreover, highly active heterojunction mesoporous ZnO/Co_3O_4 has been fabricated based on as-prepared ultra-small Co_3O_4 nanocrystals (*ca.* 3 nm) and mesoporous ZnO spheres by flexible impregnation technique. Profit from nano-size effect and synergistic effect of p-n heterojunction, mesoporous ZnO/Co_3O_4 exhibited excellent acetone sensing performance with high selectivity, superior sensitivity and responsiveness. Typically, 5 wt% Co_3O_4 embedded mesoporous ZnO sphere showed prominent acetone response (*ca.* 46 for 50 ppm), which was about 11.5 times higher than that in pure ZnO sensing device, and it was also endowed high cyclic stability. The nanocrystals embedded hybrid material is expected to be used as promising efficient material in the field of catalysis and gas sensing.

With the rapid development of intelligent sensor technology and nanomedicine detection, chemo-resistive gas sensors have aroused extensive concerns on food security, environmental protection and medical science, *etc.* [1–3]. Metal oxide semiconductors as sensitive sensing material have been exploited for decades and successfully detected multiple gases, such as flammable, disease indicator, toxic and explosive gases [4,5]. Transition traditional metal oxides possess tunable electronic structure and metal-oxygen active sites, which is beneficial for the surface adsorption of targeted gases, but their bulk structure and morphology limit to their applications due to low surface area and weak mass transfer efficiency. By contrast, mesoporous metal oxides possess better structure features, including high porosity, large specific surface area, efficient mass transfer and diffusion rate, which are extremely favorable for gas-solid interface interaction for improved gas sensing application [6,7].

In recent years, emerging mesoporous metal oxides, such as WO_3 [8], TiO_2 [9], In_2O_3 [10], SnO_2 [11], have been designed based on hard and soft template synthesis method, and it showed great application potential for detecting various toxic or explosive gases, such as H_2S, CO and butanol. Among these mesoporous metal oxides, mesoporous ZnO as typical n-type semiconductor has low crystallization temperature and wide bandgap (*ca.* 3.37 eV), which has been widely applied in catalysis [12], gas sensor [13] and solar cell [14]. For gas sensing application, ZnO is one of the earliest discovered and the most widely used oxide-based materials [15]. However, single component mesoporous ZnO usually suffers poor responsiveness and weak selectivity due to its own electronic structure and surface defect. Multicomponent mesoporous

* Corresponding author at: Department of Chemistry, State Key Laboratory of Molecular Engineering of Polymers, Shanghai Key Laboratory of Molecular Catalysis and Innovative Materials, iChEM, Fudan University, Shanghai 200433, China.
** Corresponding author.
E-mail addresses: zouyidong217@126.com (Y. Zou), yhdeng@fudan.edu.cn (Y. Deng).

https://doi.org/10.1016/j.cclet.2020.10.041
1001-8417/

ZnO-based oxides cannot only take the advantages of each component but also provide abundant heterogeneous interfaces or active sites to achieve improved sensing performance. Various methods, including element doping, nanoparticle embedding and recombination, have been applied to fabricate multicomponent ZnO-based materials [6,16,17]. In general, noble metal (*e.g.*, Au, Pt, Ag, Rh and Pd) as activity catalyst or sensitizer can significantly enhance reactivity and adsorption capacity of surface molecules (*e.g.*, O^{2-}, O^{-}, O^{2-}). Kim *et al.* [18] synthesized novel ZnO nanorods coated with amorphous Pd layer, and the obtained amorphous Pd/ZnO nanorods sensor exhibited an improved sensing response toward H_2, making them good candidate for development of H_2 gas sensor with high sensitivity and selectivity for detecting low-concentration H_2. Except for expensive noble-metal/metal-oxide based sensor, heterojunction provides a new direction for intelligent sensor, and heterojunction-based metal oxide composites (*e.g.*, n-n, p-n or p-n-p) have recently emerged as sensing components for intelligent gas sensors, and they exhibit improved electrical properties and reduced surface energy by virtue of their favorable interfacial effect and energy band structure. Taking ZnO based heterojunction materials as examples, various multiple ZnO-based heterojunction nanomaterials have been designed, such as ZnO/SnO_2, ZnSe/ZnO. For example, Huang *et al.* [19] demonstrated n-p-n ZnO-based heterojunction, which existed in the contact region between SnO_2 nanorods and ZnO thin layer. SnO_2 nanorod arrays were fabricated *via* plasma-enhanced CVD method and then coated a layer of ZnO on the surface of SnO_2 nanorods. The ZnO/SnO_2 nanorod sensor exhibits a normal n-type response to CH_4, NH_3 and CO but it shows a special concentration-dependent n-p-n transition in sensing response to H_2. Similarly, Liu *et al.* [20] fabricated mesoporous ZnSe/ZnO heterojunctions by the in-situ thermal oxidation of ZnSe in air, where the ZnSe/ZnO heterojunction-based sensor showed superior NO_2 sensing performance than pure ZnO owing to its novel mesoporous structure and the formation of heterojunctions.

As common p-type semiconductor, Co_3O_4 possesses narrow indirect band gap (1.5 eV) and prominent catalytic activity, and it has been widely explored in various applications such as catalysts [21], electrode materials [22,23] and gas sensors [22]. Specially, Co_3O_4 can be used as active component (Co^{3+} and oxygen vacancies) to enhance the selectivity and gas response in gas sensor. It is well-known that minimize the size of sensing materials can enhance surface activity for physical adsorption or chemical reaction, which is favorable for the extension of depletion layer and surface reaction of oxygen species. Previous studies have shown that faster charge transfer can induce higher electron-hole separation efficiency when the heterojunction is as small as 2−3 nm [24,25]. Therefore, it is very important to develop reliable method for loading ultra-small metal oxide nanoparticles on other semiconductor metal oxides to improve charge separation efficiency.

Herein, unique mesoporous ZnO spheres with high surface area and tunable mesopores were synthesized *via* a formaldehyde-assisted metal-ligand crosslinking strategy, and these mesoporous ZnO spheres possess uniform size and high porosity. Ultra-small Co_3O_4 nanocrystals (~3 nm) were embedded in the mesopores of ZnO spheres to enhance the electron-hole separation efficiency. Importantly, the obtained mesoporous ZnO/Co_3O_4 composites exhibit excellent gas sensing performance towards acetone compared with pure mesoporous ZnO spheres. The response of 5 wt% Co_3O_4 embedded mesoporous ZnO sphere composites to 50 ppm acetone reached 46 at 250 °C, which was about 11.5 times higher than that of pure ZnO under the same condition due to the formation of mesoporous p-n heterojunctions at the interface of ZnO and Co_3O_4.

Metal-phenolic coordination spheres were synthesized by novel formaldehyde-assisted metal-ligand crosslinking strategy according to reported previously [26,27], and uniform ZnO spheres with abundant mesopores could be obtained after calcination treatment for the removal of organic species. Based on the strong metal-chelating interaction, a series of multi-component metallic spheres can be synthesized, such as single, binary and multiple. In this study, pre-synthesized Co_3O_4 nanocrystals were encapsulated into the pores of mesoporous ZnO spheres through facile and simple impregnation technique, and ultra-small Co_3O_4 nanocrystals could be deposited in the mesopores of ZnO spheres to provide enormous ZnO/Co_3O_4 interfaces. The whole synthesis process for mesoporous ZnO/Co_3O_4 spheres was schematically shown in Scheme 1. TA ($C_{76}H_{52}O_{46}$) is a kind of plant polyphenol with five galloyl groups and five catechol groups, which can chelate with various metal ions. Tannic acid acts as a skeleton template in the synthesis, the addition of TA is important to adjust the morphology and structure of metal-phenolic coordination polymers. In the polymerization process, TA molecules were firstly crosslinked by formaldehyde to produce composite resin under alkaline conditions, and then metal-TA coordination spheres were formed *via* the strong metal-ligand coordination interactions between Zn^{2+} ions and catechol groups of polymer oligomers. After calcination in air at 400 °C for 2 h, uniform mesoporous ZnO spheres were obtained. In order to acquire highly active mesoporous ZnO/Co_3O_4 composites, the pre-synthesized ultra-small Co_3O_4 nanocrystals (3.0 nm) and mesoporous ZnO spheres were dispersed in ethanol under vigorous stirring in air, and the nanocrystals could diffuse into the pores by the capillary effect of mesopores during evaporation of ethanol. The resultant mesoporous ZnO/Co_3O_4 composites were annealed at 300 °C in air to enable the strong $ZnO\text{-}Co_3O_4$ interaction.

Transmission electron microscopy (TEM) images indicate that the Zn-TA coordination nanospheres have uniform spherical structure with smooth surface. Taking ZnO-50 as an example, the as-made Zn-TA coordination spheres have average diameter of 180 nm (Figs. 1a and b), and after calcination in air the obtained mesoporous ZnO spheres exhibit rough morphology and abundant ZnO grains with high crystallinity, which can produce disordered grain accumulation pores (Figs. 1c and d). As shown in Fig. S1 (Supporting informatoin), a series of mesoporous spherical ZnO spheres with various properties (*e.g.*, pore size, surface area, surface roughness) can be also obtained *via* the same synthesis process by adjusting the weight percentage of zinc salts to TA added in the reaction system.

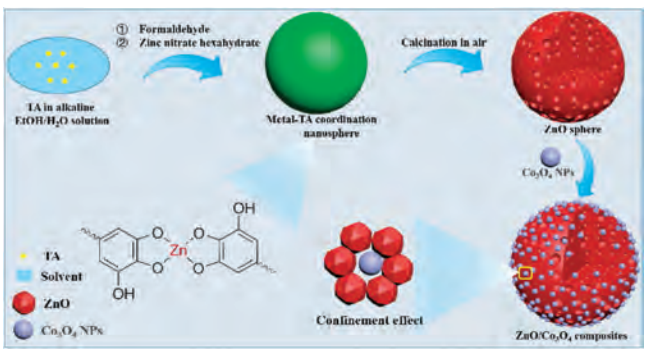

Scheme 1. The synthesis pathway for mesoporous ZnO/Co_3O_4 composites. Step 1. In the polymerization process, TA molecules were firstly crosslinked by formaldehyde to produce composite resin under alkaline conditions, and then metal-TA coordination spheres were formed *via* the strong metal-ligand coordination interactions between Zn^{2+} ions and catechol groups of polymer oligomers. Step 2. The as-prepared organic-inorganic composites were calcined in air at 400 °C for 2 h with a ramp of 2 °C/min, forming crystalline mesoporous ZnO spheres. Step 3. A complete evaporation of ethanol and the deposition of Co_3O_4 nanocrystals in the mesopores of ZnO spheres to obtain mesoporous ZnO/Co_3O_4 composites.

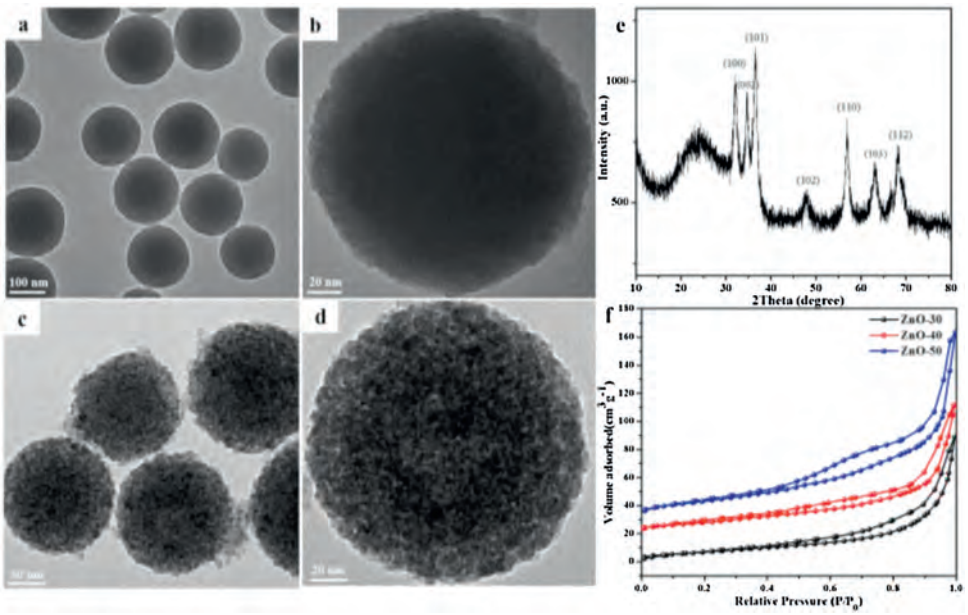

Fig. 1. TEM images of (a, b) Zn-TA-50 coordination spheres; (c, d) ZnO-50 spheres. (e) XRD pattern of mesoporous ZnO-50 spheres. (f) N_2 adsorption-desorption isotherms of mesoporous ZnO-X spheres recorded at 77 K (samples with X of 30, 40 and 50 were offset vertically by 0, 20 and 30 cm^3/g, respectively).

The X-ray diffraction (XRD) pattern of mesoporous ZnO-50 (Fig. 1e) exhibits well-resolved peaks at 2θ of 32.1°, 34.6°, 36.5°, 47.7°, 56.9°, 63.1° and 68.2°, which are corresponding to the ZnO crystal planes of (100), (002), (101), (102), (110), (103) and (112), respectively. Small-angle X-ray scattering (SAXS) patterns of ZnO samples exhibit no obvious scattering peaks, indicating its disordered structure (Fig. S2 in Supporting information), which is consistent with the results of TEM image.

N_2 adsorption-desorption isotherms of all as-prepared samples show sharp capillary condensation steps in the relative pressure range of 0.90−0.98 (Fig. 1f) and the pore size as well as specific surface area is shown in Table S1 (Supporting information). For mesoporous ZnO, the surface area increases from 24.95 m^2/g to 51.06 m^2/g with the increase of zine salts and all as-prepared ZnO spheres has adjustable pore size based on Barrett-Joyner-Halanda (BJH) model, which indicates there is typical mesoporous structure produced by the accumulation of ZnO grains. Especially, according to the pore size distribution of ZnO (Fig. S3 in Supporting information), there is a weak peak for larger pore size (9.9 nm for ZnO-30, 7.4 nm for ZnO-40 and 11.8 nm for ZnO-50), which can provide abundant adhere sites for ultra-small Co_3O_4 nanocrystals (~3 nm).

According to the above discussion, the obtained ZnO spheres have an attracted mesoporous structure, which is suitable for loading ultra-small Co_3O_4 nanocrystals into the pore channels, so as to construct p-n heterojunctions to improve the gas sensing properties of the composites. Therefore, ZnO/Co_3O_4 composites were synthesized by impregnation method and their gas sensing properties were studied. It can be seen from the TEM images of ZnO-50-Co_3O_4-5% composites (Fig. S4 in Supporting information) that the morphology of ZnO without change significantly after loading Co_3O_4 nanocrystals by impregnation method. The HRTEM image of Co_3O_4 nanocrystals (Fig. S5a in Supporting information) exhibits obvious crystal lattice and the selected area electron diffraction (SAED) analysis reveals diffraction rings, which indicates that these as-prepared Co_3O_4 nanocrystals possess pre-crystallization feature. Due to their ultrasmall size features, these ultra-small Co_3O_4 nanocrystals can not only provide nano-size effect to accelerate mass transfer but also enhance catalytic effect in the process of gas sensing reaction. By contrast, the HRTEM image of ZnO-50-Co_3O_4-5% (Fig. S5b in Supporting information) shows that there is no obvious crystal lattice for Co_3O_4 nano-crystals while it shows [100] lattice fringe of ZnO clearly, which is due to its ultra-small size and overspread effect of highly crystalline ZnO. The STEM image (Fig. S5c in Supporting information) and element mapping (Figs. S5d-f in Supporting information) of above composite shows a homogeneous distribution of Zn, O and Co, and highly dispersed Co_3O_4 nanoparticles are encapsulated in the pores of mesoporous ZnO.

The XRD patterns of mesoporous ZnO/Co_3O_4 composites are shown in Fig. 2a, and it can be clearly seen the well-resolved peaks of ZnO. Fig. S6 (Supporting information) shows a typical XRD pattern of Co_3O_4. The diffraction peaks at 19.0°, 36.9°, 44.9°, 59.6° and 65.3° can be indexed to (111), (311), (400), (511) and (440) (JCPDS No. 74-1656), respectively. However, there is still no obvious diffraction peaks of Co_3O_4 nanocrystals in the XRD patterns of ZnO/Co_3O_4 composites, which might be due to the low content of Co_3O_4 nanocrystals in the composites and ultra-small size of Co_3O_4 nanoparticles (~3 nm). Although the peak of Co_3O_4 species cannot be observed in the XRD pattern, the presence of Co element can be observed in the EDS pattern (Fig. S7 in Supporting information). ICP analysis was also carried out to evaluate the content of Co element in ZnO/Co_3O_4 composites, as shown in Table S2, which further confirms the existence of Co element. According to the FT-IR spectra of ZnO and ZnO/Co_3O_4 composites (Fig. 2b), the strong peak around 460 cm^{-1} is corresponding to the stretching mode of Zn-O bonds (ZnO species) [28]. The weak peak at 660 cm^{-1} demonstrates the existence of the Co_3O_4 nanocrystals, which is related to the stretching vibrations of the metal-oxygen bonds (Co-O) [29,30].

As shown in Fig. 2c, the Raman spectra of mesoporous ZnO and mesoporous ZnO/Co_3O_4 composites exhibits similar characteristic peaks, and the position of peaks without obvious changes after the incorporation of Co_3O_4 nanocrystals. But the intensity of the peak decreases with the increase of Co_3O_4 nanocrystals, indicating a certain interaction between ZnO grains and ultra-small Co_3O_4 nanocrystals. In ZnO/Co_3O_4 composites, since the Fermi level of ZnO sphere is higher than that of Co_3O_4, electrons will transfer from ZnO grain to Co_3O_4 nanocrystals until their Fermi level is balanced, and more defects are generated. When the amount of

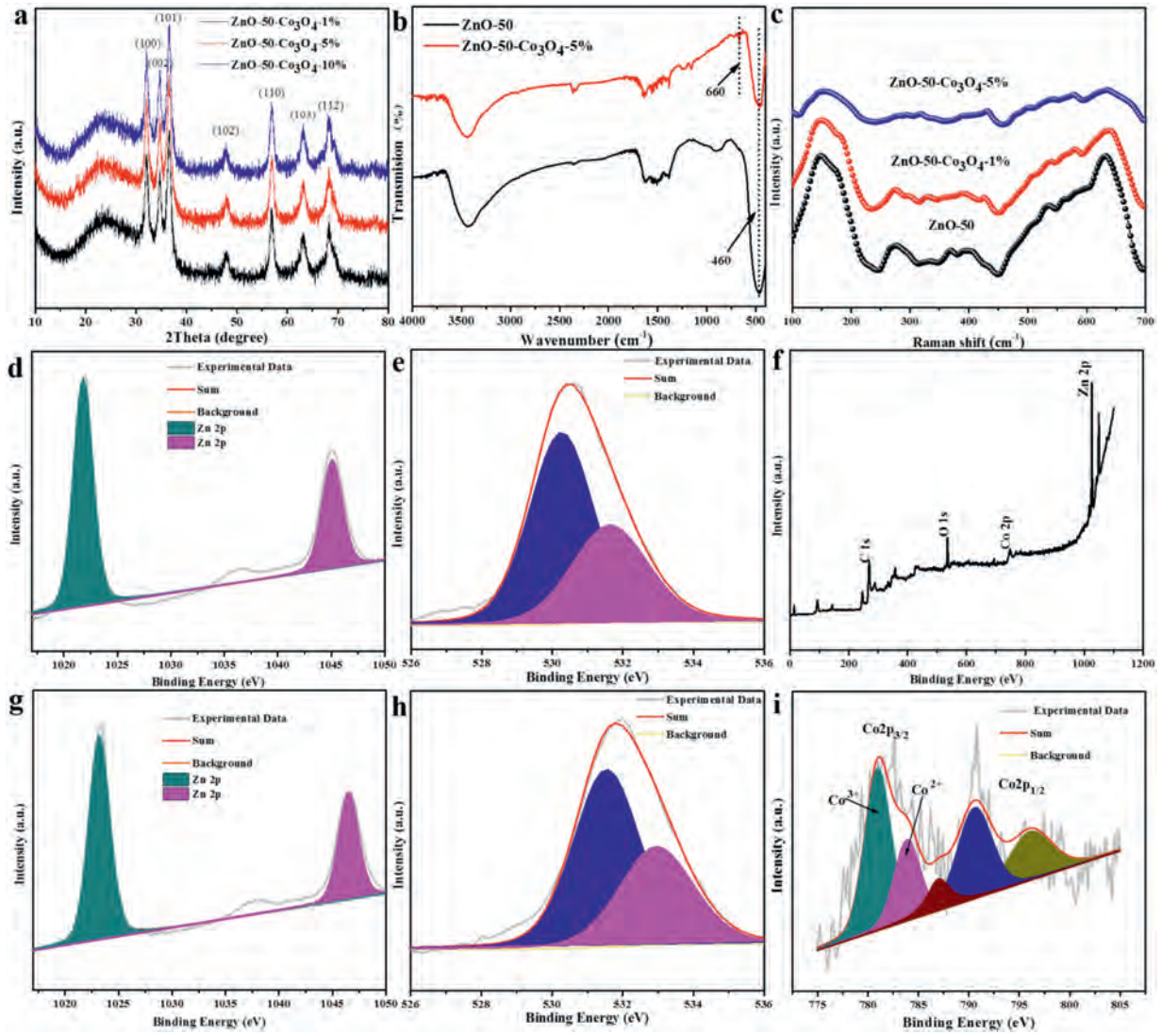

Fig. 2. (a) XRD patterns, (b) FTIR spectra, (c) Raman spectra of mesoporous ZnO and mesoporous ZnO/Co_3O_4 composites. Zn 2p XPS spectra of (d) ZnO and (g) ZnO-50-Co_3O_4-5%. O 1s XPS spectra of (e) ZnO and (h) ZnO-50-Co_3O_4-5%. (f) XPS full survey of ZnO-50-Co_3O_4-5%. (i) Co 2p XPS spectra of ZnO-50-Co_3O_4-5%.

Co_3O_4 nanocrystals increased, the more crystal defects are produced and the vibration stretching strength of the Zn-O bond will decrease, which will lead to the weakening of the Raman peak intensity. Similarly, N_2 adsorption-desorption isotherms of all ZnO/Co_3O_4 samples also show sharp capillary condensation steps in the relative pressure range of 0.90−0.98 (Fig. S8 in Supporting information), where the pore size and specific surface area are shown in Table S3 (Supporting information). The specific surface area of ZnO-50-Co_3O_4-X decreases with the increase of Co_3O_4 content and the pore size of the ZnO/Co_3O_4 composites decreases obviously compared with ZnO-50, which mainly due to the pore encapsulation of mesoporous ZnO spheres by ultra-small Co_3O_4 nanocrystals.

XPS analysis was performed to investigate the chemical states of the mesoporous ZnO/Co_3O_4 composites. As shown in Fig. 2f, it confirms the presence of four elements (Zn, O, Co and C). The narrow-scan Zn 2p spectrum can be assigned to Zn $2p_{3/2}$ (1023.2 eV) and Zn $2p_{1/2}$ (1046.5 eV) (Fig. 2g), respectively, which indicates that the coordination form and chemical valence of Zn^{2+} in ZnO/Co_3O_4 composites is normal [31]. By contrast, the peak positions of Zn 2p spectrum for above composites exhibit a higher binding energy than pure mesoporous ZnO (Fig. 2d) (Zn $2p_{3/2}$ at 1021.8 eV and Zn $2p_{1/2}$ at 1045.1 eV), which reveals that Co_3O_4 nanocrystals can interact with ZnO grains and accelerate electron transfer rate [32]. This kind of shift is generally induced by the change of coordinated environment or chemical state [33]. Similarly, the XPS spectra of O1s (Figs. 2e and h) can be divided into two different oxygen species (such as adsorbed oxygen and lattice oxygen). The peaks at ~ 531.0 and 532.0 eV are assigned to the crystal lattice oxygen (O^{2-}) and the surface-absorbed oxygen (O^{2-} or O^{-}), respectively. Interestingly, there is typical migration of peak position, which is attributed to the doping of Co_3O_4 nanocrystals, and it can affect the coordination environment or metal-oxygen bonds (*i.e.*, Co-O and Zn-O). The Co 2p XPS spectra of ZnO-50-Co_3O_4-5% shows two major peaks at 780.0 eV and 790.7 eV, which is corresponding to the Co $2p_{3/2}$ and Co $2p_{1/2}$ spin-orbit peaks of Co_3O_4 species, respectively (Fig. 2i). In addition, a weak satellite peak at around 787.2 eV can be clearly detected, which is further confirmed the existence of Co_3O_4 nanocrystals [34].

Mesoporous ZnO is regarded as efficient semiconductor sensing material, and Co_3O_4 nanocrystals can further optimize material performance. Thus, the sensing properties of the composite were evaluated systematically. The electric circuit for measuring and the assembled sensing device are demonstrated in Fig. 3a, where R_f is represented as the reference resistor and R_x is the resistor of

material to be tested, V_o is the output voltage and I_x is the current. It can be clearly seen that the gas-sensing properties of semiconducting metal oxides is closely related to the operating temperature. To optimize the operating temperature, the mesoporous ZnO/Co_3O_4 composites sensors were tested towards 50 ppm of acetone at 150−350 °C. As shown in Fig. 3b, the response value for pure mesoporous ZnO spheres increased slowly with the increase of working temperature, while it still maintained low response value (< 5.0) even under 350 °C. The poor acetone sensing performance of pure mesoporous ZnO spheres is related to electronic structure and optoelectronic properties. By contrast, under the assistance of ultra-small Co_3O_4 nanocrystals, the response value to acetone under same condition increased first and then decreased with the changing of working temperature. The optimum sensing temperature is near 250 °C, which can be attributed to the high dispersion of Co_3O_4 nanocrystals and the formation of ZnO-Co_3O_4 heterostructures. Moreover, the response value increased gradually from ZnO-30-Co_3O_4-5% to ZnO-50-Co_3O_4-5%, which can be explained by the pore volume and specific surface area increased from ZnO-30 to ZnO-50 (as shown in Fig. S3 and Table S1). More importantly, the response value of ZnO-50-Co_3O_4-5% to 50 ppm acetone reached 46 at 250 °C, which is 11.5 times higher than that of pure mesoporous ZnO-50 (response value = 4.0) under the same condition. Compared with ZnO/Co_3O_4 materials reported previously (Table S4 in Supporting information), the mesoporous ZnO/Co_3O_4 composites exhibited great potential in acetone gas sensor due to its relative low operating temperature and high sensitivity. As shown in Fig. 3c, a series of common volatile gases, such as toluene, ammonia, methane, formaldehyde, carbon monoxide and hydrogen were chosen as the interfering gases to study the selectivity of ZnO/Co_3O_4 composites. The response of ZnO-50-Co_3O_4-5% to 50 ppm acetone was at least 13 times higher than other gases, which indicates excellent acetone selectivity. It fully indicates that the incorporation of Co_3O_4 nanoparticles is very helpful to improve the gas sensing properties of the materials. In addition, the advantages of the impregnation method can also be seen from Fig. 3d. The response value of ZnO/Co_3O_4 composites *via* the impregnation method was much higher than pure mesoporous ZnO spheres (4.0) and Co_3O_4 nanocrystals (1.66) to 50 ppm acetone at 250 °C. The enhanced gas sensing performance of ZnO/Co_3O_4 composites was mainly ascribed to the formation of p-n heterojunctions between ZnO grains and Co_3O_4 nanocrystals, which greatly increased the baseline resistance in air and reduced the resistance in acetone gas. Therefore, a larger variation of resistance produced when converting from air to acetone atmosphere. According to the definition of response (R_a/R_g), the response to acetone increased a lot. The response of ZnO/Co_3O_4 composites *via* the impregnation method increased first and then decreased with the increase of the amount of Co_3O_4, and reached a maximum when the amount of Co_3O_4 was 5%. It is attributed to that the number of reactive sites increases with the increase of the amount of Co_3O_4 nanocrystals, and more reactive sites can provide abundant adhere sites for oxygen species (*i.e.*, O_2^-, O^- and O^{2-}). However, when the amount of Co_3O_4 continues to increase, the agglomeration of Co_3O_4 nanoparticles will occur and the overloading of Co_3O_4 nanocrystals can block the pores, which can restrain the fast gas molecules penetration and efficient interior electron transport. Therefore, the response value will decrease again, which can be confirmed by the fact that the specific surface area of ZnO-50-Co_3O_4 decreased with the increase of Co_3O_4 content (as shown in Fig. S8 and Table S3). This experimental result indicates that the incorporation of Co_3O_4 nanoparticles greatly improves the response of ZnO spheres to acetone, which mainly due to the formation of heterojunctions and more active sites of the post-loaded complex are exposed to the targeted gas. Moreover, previous studies have shown that faster charge transfer leads to higher electron-hole separation efficiency when the heterojunction is as small as 2−3 nm [24,25]. Thus, smaller nanocrystals are

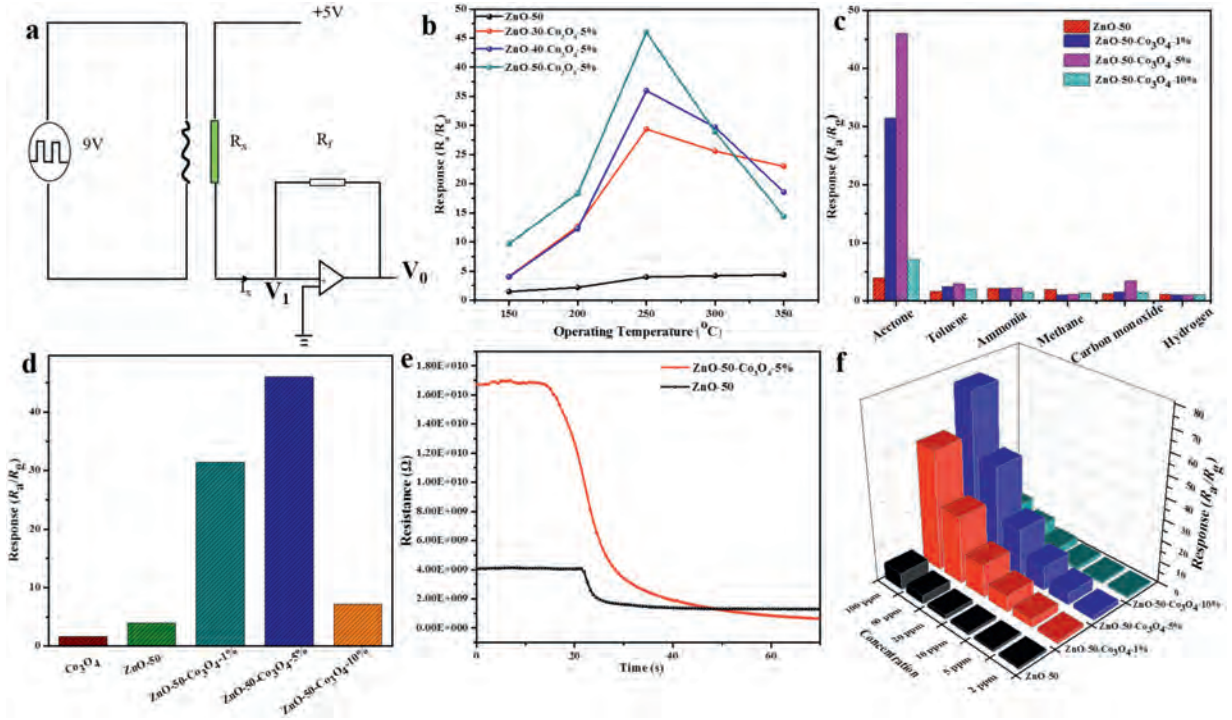

Fig. 3. (a) The electric circuit for measuring. (b) Responses of the sensors to 50 ppm acetone at different working temperature (150-350 °C). (c) Selectivity of ZnO and ZnO/Co_3O_4 composites sensors to various gases at 50 ppm at 250 °C. (d) Responses of ZnO, Co_3O_4 and ZnO-50-Co_3O_4-*X* (*X* = 1%, 5% and 10%) towards 50 ppm acetone at 250 °C. (e) Response of ZnO and ZnO-50-Co_3O_4-5% composite sensor upon exposure to 50 ppm of acetone at 250 °C. (f) Gas response towards different concentration of acetone of ZnO and ZnO/Co_3O_4 composites at 250 °C.

beneficial for gas sensing application, and more attentions should be focused on the design of ultra-small heterojunctions. Moreover, the base resistance of the ZnO changed accordingly after the incorporation of Co_3O_4 nanoparticles (Fig. 3e), which confirms the existence of a wider range of depletion layers proposed by p-n junction.

The dynamic gas sensor responses of ZnO/Co_3O_4 composites and pure mesoporous ZnO spheres to different concentrations of acetone from 2.0 ppm to 100 ppm are shown in Fig. 3f and Fig. S9a (Supporting information). With the increase of acetone concentration, the response of ZnO-50-Co_3O_4-5% sensor increased from 2.2 at 2 ppm to 75 at 100 ppm, which exhibited a much higher sensitivity than pure mesoporous ZnO-50 spheres. Fig. S9b (Supporting information) shows the response of ZnO-50-Co_3O_4-5% sensor to different acetone concentrations ranging from 0.2 ppm to 1 ppm, and a response of 1.18 is realized at an acetone concentration of 0.2 ppm. The high sensitivity is attributed to the larger specific surface area and the formation of smaller heterojunction sites. The ZnO-50-Co_3O_4-5% sensor showed a fast response of 60 s when exposed to 50 ppm acetone (Fig. S9c in Supporting information). In addition, the sensor exhibited a good cycle performance towards 50 ppm acetone (Fig. S9d in Supporting information), indicating good stability for the sensitive detection of acetone.

The sensing performance of the ZnO/Co_3O_4 composites was tested on a platform based on a side-heated type of gas sensor and the interaction between ZnO/Co_3O_4 composites and acetone molecules was shown in Fig. 4a. The sensing mechanism of ZnO sphere follows the surface-resistance controlled model, and the resistance change of ZnO is relevant to the amount and species of chemisorbed oxygen (*i.e.*, O_2^-, O^- or O^{2-}) in the process of adsorption and desorption. When ZnO sensor is exposed to air, oxygen molecules will be adsorbed on the surface of ZnO sphere and capture electrons from the conduction band of ZnO sphere to form oxygen species (as Eqs. 1–4), which leads to the formation of a depletion layer on the surface of bare ZnO [35]. When exposed to acetone gas, O^{2-} and O^- species can react with the acetone gas molecules and release electrons back to the conduction band of ZnO sphere. Therefore, the depletion layer becomes thin and the resistance of sensor decreases.

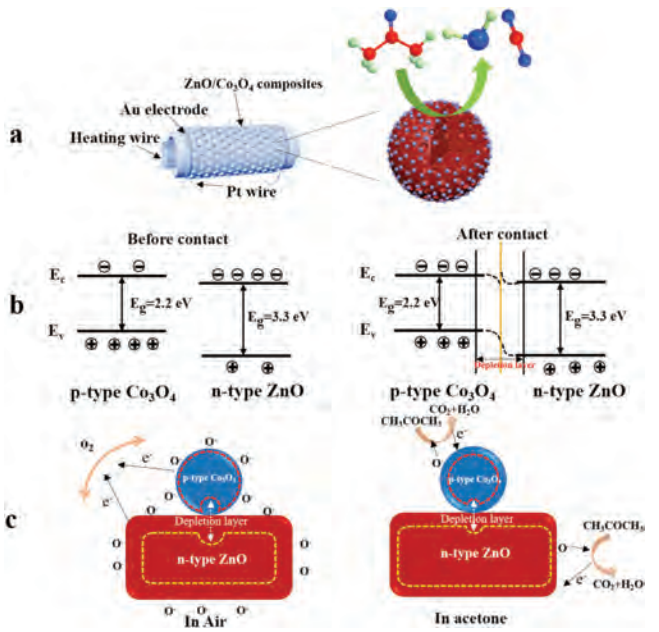

Fig. 4. (a) Sketch of the structure of side-heated gas sensor based on ZnO/Co_3O_4 composites and diagram of the interaction between ZnO/Co_3O_4 composites and acetone molecules. (b) Band diagrams of ZnO grain and Co_3O_4 nanocrystal before contact and after contact and (c) schematic diagram of the mechanism of ZnO/Co_3O_4 composites for acetone-gas sensing.

$$O_2(gas) \rightarrow O_2\ (ads) \quad (1)$$

$$O_2(ads) + e^- \rightarrow O_2^-\ (ads) \quad (2)$$

$$O_2^-(ads) + e^- \rightarrow 2O^-\ (ads) \quad (3)$$

$$CH_3COCH_3(gas) + 6O^-(ads) \rightarrow 3CO_2 + 3H_2O + 6e^- \quad (4)$$

However, after loading with Co_3O_4 nanocrystals, the working temperature for the sensors decreased and the response value to acetone has also been greatly improved, which can be attributed to the excellent catalytic performance of highly dispersed Co_3O_4 nanocrystals and the formation of ZnO/Co_3O_4 p-n heterostructure. The porous structure makes it possible to deposit more Co_3O_4 nanocrystals in the pores of mesoporous ZnO, which can induce that the gas sensing reaction takes place uniformly in the whole mesoporous ZnO spheres.

The energy band structure of ZnO grain and Co_3O_4 nanocrystal before contact and after contact is shown in Fig. 4b. As we all know, the conductivity behaviors of p-type Co_3O_4 is completely opposite to that of n-type ZnO spheres. In ZnO/Co_3O_4 heterostructure, since the Fermi level of ZnO sphere is higher than that of Co_3O_4, electrons will transfer from ZnO grain to Co_3O_4 nanocrystals, which leads to the band bending and an additional depletion layer (electronic depletion on the surface of ZnO, while hole depletion on the surface of Co_3O_4) until their Fermi level is balanced, as shown in Figs. 4b and c. P-N Heterojunctions are formed at the interface between ZnO nanoparticles and Co_3O_4 nanocrystals [36], and the recombination of electrons and holes significantly decreases the charge conduction channel and leads to a higher resistance than pure ZnO (the base resistance of ZnO and ZnO-50-Co_3O_4-5% were shown in Fig. 3e and Table S5 in Supporting information). Moreover, since the content of Co_3O_4 is relatively small in ZnO/Co_3O_4 composites, the p-n heterojunction and conductivity of mesoporous ZnO spheres still play an important role. When it exposed to acetone gas, electrons trapped by oxygen species are released back to ZnO grains, leading to an increase of electron concentration and a decrease in the sensor resistance. Therefore, according to the response definition of R_a/R_g, the response of ZnO/Co_3O_4 composites in acetone gas is significantly enhanced due to the formation of a deeper electron depletion layer.

In this work, ZnO nanospheres and ZnO/Co_3O_4 composites were synthesized by a facile and efficient method, which possess typical spherical structure with high specific surface area, abundant pores and highly dispersed grains. In addition, the pore structure of mesoporous ZnO can be adjusted by changing the weight percentage of zinc salt to TA added in the reaction system and Co_3O_4 nanocrystals were deposited into mesopores of mesoporous ZnO by virtue of the capillary effect in the process of solvent evaporation. The obtained ZnO/Co_3O_4 composites exhibited excellent acetone sensing performance, and the optimum response value of mesoporous ZnO/Co_3O_4 composites to 50 ppm acetone reached 46 at 250 °C, which is 11.5 times higher than that of pure ZnO spheres (4.0) under the same condition. Moreover, the enhanced response of ZnO/Co_3O_4 composite sensor to acetone is attributed to the existence of p-n heterojunction between ZnO grains and Co_3O_4 nanocrystals. This research provides a reasonable way for the design of chemical resistance gas sensor with high performance.

Declaration of competing interest

The authors report no declarations of interest.

Acknowledgments

This work was financially supported by the National Natural Science Foundation of China (Nos. 21673048, 21875044, 52073064, 22005058 and 22005057), National Key R&D Program of China (No. 2018YFA0209401), Key Basic Research Program of Science and Technology Commission of Shanghai Municipality (No. 20JC1415300), Program of Shanghai Academic Research Leader (No. 19XD1420300), and the state key laboratory of Transducer Technology of China (No. SKT1904) The authors thank to research supporting project number (No. RSP-2020/155), King Saud University, Riyadh, Saudi Arabia.

Appendix A. Supplementary data

Supplementary material related to this article can be found, in the online version, at doi:https://doi.org/10.1016/j.cclet.2020.10.041.

References

[1] A. Dey, Mater. Sci. Eng. B 229 (2018) 13282–13289.
[2] A.T. Guntner, N.J. Pineau, P. Mochalski, et al., Anal. Chem. 90 (2018) 4940–4945.
[3] M. Righettoni, A. Amann, S.E. Pratsinis, Mater. Today 18 (2015) 163–171.
[4] Y.H. Li, W. Luo, N. Qin, et al., Angew. Chem. Int. Ed. 53 (2014) 9035–9040.
[5] T. Zhao, Y. Ren, G.Y. Jia, et al., Chin. Chem. Lett. 30 (2019) 2032–2038.
[6] S.W. Qin, P.G. Tang, Y.J. Feng, et al., Sens. Actuator. B: Chem. 309 (2020) 1278001.
[7] X.Y. Yang, X.W. Cheng, J.H. Ma, et al., Small 15 (2019) 1903058.
[8] Y.H. Li, X.R. Zhou, W. Luo, et al., Adv. Mater. Interfaces 6 (2018) 1801269.
[9] T.J. Ha, M.H. Hong, C.S. Park, et al., Sens. Actuator. B: Chem. 181 (2013) 874–879.
[10] G.X. Zhu, L.J. Guo, X.P. Shen, et al., Sens. Actuator. B: Chem. 220 (2015) 977–985.
[11] X.Y. Xiao, L.L. Liu, J.H. Ma, et al., ACS Appl. Mater. Interfaces 10 (2018) 1871–1880.
[12] R.Z. Zhang, J.W. Jiang, J.P. Zhou, et al., Adv. Mater. 30 (2018) 1705443.
[13] N. Zhang, L.M. Yan, Y. Lu, et al., Chin. Chem. Lett. 31 (2020) 2071–2076.
[14] P. Labouchere, A.K. Chandiran, T. Moehl, et al., Adv. Energy Mater. 4 (2014) 1400217.
[15] J.Q. Xu, J.J. Han, Y. Zhang, et al., Sens. Actuator. B: Chem. 132 (2008) 334–339.
[16] X.R. Zhou, Y.D. Zou, J.H. Ma, et al., Chem. Mater. 31 (2019) 8112–8120.
[17] Y.L. Zhang, C.W. Jia, Q. Kong, et al., ACS Appl. Mater. Interfaces 12 (2020) 26161–26169.
[18] H. Kim, Y. Pak, Y. Jeong, et al., Sens. Actuator. B: Chem. 262 (2018) 460–468.
[19] H. Huang, H. Gong, C.L. Chow, et al., Adv. Funct. Mater. 21 (2011) 2680–2686.
[20] W. Liu, D. Gu, X.G. Li, ACS Appl. Mater. Interfaces 11 (2019) 29029–29040.
[21] Y.N. Qin, Y.J. Sun, Y.J. Li, et al., Chin. Chem. Lett. 31 (2020) 774–778.
[22] W.Y. Li, L.N. Xu, J. Chen, Adv. Funct. Mater. 15 (2005) 851–857.
[23] X.W. Lou, D. Deng, J.Y. Lee, et al., Adv. Mater. 20 (2008) 258–262.
[24] L.C. Liu, Z.Y. Ji, W.X. Zou, et al., ACS Catal. 3 (2013) 2052–2061.
[25] W.A. Tisdale, K.J. Williams, B.A. Timp, et al., Science 328 (2010) 1543–1547.
[26] G. Wang, X.R. Zhou, Y.H. Deng, et al., Adv. Funct. Mater. 28 (2018) 1806144.
[27] J. Wei, G. Wang, F. Chen, et al., Angew. Chem. Int. Ed. 57 (2018) 9838–9843.
[28] A.E. Jimenez-Gonzalez, J.A.S. Urueta, R. Suarez-Parra, J. Cryst. Growth 192 (1998) 430–438.
[29] Y.J. Liu, G.X. Zhu, B.L. Ge, et al., CrystEngComm 14 (2012) 6264–6270.
[30] X.H. Xia, J.P. Tu, Y.Q. Zhang, et al., RSC Adv. 2 (2012) 1835–1841.
[31] C.J. Dong, X.C. Xiao, G. Chen, et al., Mater. Chem. Phys. 155 (2015) 1–8.
[32] M. Rakibuddin, R. Ananthakrishnan, RSC Adv. 5 (2015) 68117–68127.
[33] B.J. Jiang, C.G. Tian, Q.J. Pan, et al., J. Phys. Chem. C 115 (2011) 23718–23725.
[34] T. He, D.R. Chen, X.L. Jiao, et al., Chem. Mater. 17 (2005) 4023–4030.
[35] Z.H. Wang, J. Xue, D.M. Han, et al., ACS Appl. Mater. Interfaces 7 (2015) 308–317.
[36] Z.K. Xu, G.T. Duan, Y. Li, et al., Chemistry 20 (2014) 6040–6046.